High-contrast spectroscopy of exoplanet atmospheres

Landman, R.

1 Introduction

1.1 The exoplanet revolution

The pursuit of understanding our cosmic origins has been a central theme throughout human history. From the ancient Greeks to the Renaissance, the existence of extrasolar planets and the possibility of life beyond the Earth has persistently captivated the human intellect. Over the past three decades, the field of astronomy has witnessed a significant paradigm shift, revealing a diverse population of planets beyond our Solar system. This transformative era started with the discovery of two planetary-mass objects orbiting the pulsar PSR B1257+12 by Wolszczan & Frail (1992), revealing for the first time the presence of planets beyond the gravitational reach of our Sun. A subsequent breakthrough came in 1995 by Mayor & Queloz (1995) with the discovery of 51 Pegasi b, a Jupiter-like exoplanet in an unusually close orbit around a main sequence star, eventually earning them the 2019 Nobel Prize in Physics. This type of planet, which later became known as a hot Jupiter, puzzled astronomers. The presence of such a massive planet, about half of Jupiter's mass, so close to its host star was not compatible with planet formation theory. Since then, the exoplanetary census has flourished, with the discovery of over five thousand planets using various detection methods. These exoplanets show a tremendous diversity that is not seen in the Solar system, as illustrated in the the mass-period diagram in Fig. 1.1. The current inventory of exoplanets includes a large amount of hot Jupiters, which turn out to be more common than initially expected. We have also seen a large number of super-Earths, planets with masses of a few times that of the Earth that are thought to have rocky cores (Seager et al., 2007), and mini-Neptunes, planets which could have a rocky core with a thick hydrogen/helium atmosphere but could also be water-worlds with deep oceans (Bean et al., 2021). Moreover, we are starting to find a growing number of super-Jupiters, massive planets on very wide orbits that span the planet and brown dwarf boundary, which are unexpected to form so far from their host star. The vast diversity of all these exoplanets shows that the planet formation and evolution process is complex, and has a large range of outcomes. The discovery of all these different worlds raises many questions: What are these planets like? How did they form? Is there life possible on these distant worlds?

1.1.1 Indirect detection

The increasing number of detected exoplanets is a result of technological advancements in combination with clever detection methods. Most of these planets have

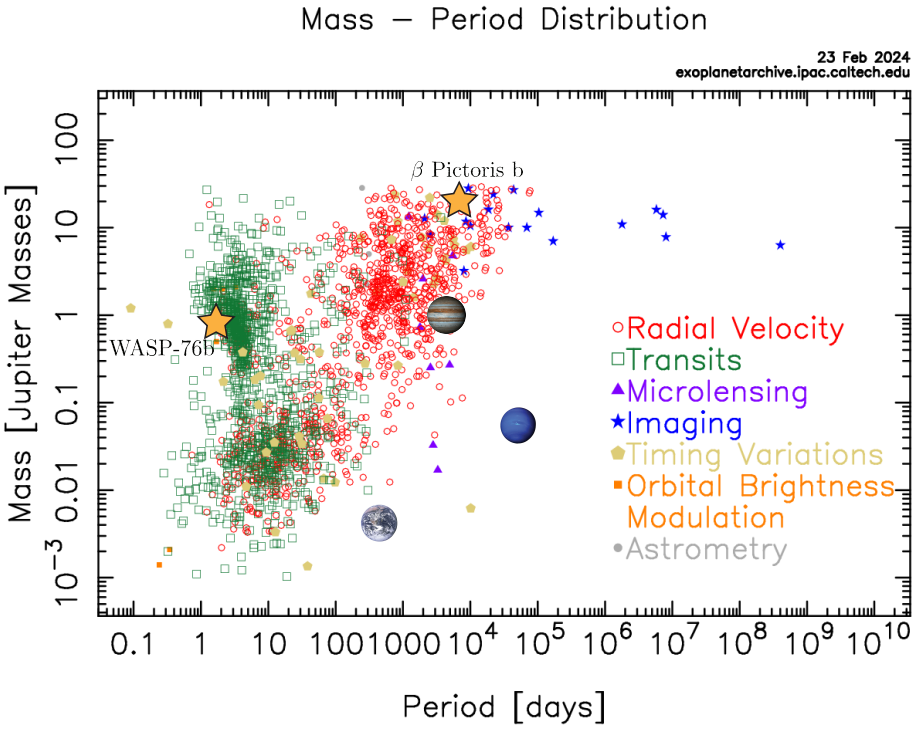

Figure 1.1: A mass versus orbital period diagram illustrating the diverse population of confirmed exoplanets as of 23 February 2024. The location of the Earth, Jupiter and Neptune is also indicated in this diagram, as well as WASP-76b and β Pictoris b, which are two of the planets studied in this thesis. Figure adapted from the NASA Exoplanet Archive.

been detected using indirect methods, where the presence of an exoplanet is inferred through an alteration of the stellar signal. By far the most successful techniques, in terms of the number of detected planets, are the radial velocity and transit method, which I will discuss in more detail below. Other indirect methods which can be used to infer the presence of an exoplanet include, for example, astrometry, where a wobble in the position of the star on the sky can be seen; microlensing, where the gravity well of the planet enhances the brightness of a background star; and pulsar timing, which was used for the detection of the objects around PSR B1257+12.

Radial velocity

The radial velocity (RV) method aims to detect stellar reflex motion induced by the gravitational pull of orbiting planets. By measuring variations in the Doppler shift of the stellar spectrum over time, it is possible to infer the presence of a planet and derive its mass and orbital period. This method was used by Mayor & Queloz (1995) for their discovery of 51 Pegasi b using the ELODIE spectrograph (Baranne et al., 1996). While initial RV surveys were mostly sensitive to close-in massive planets (hot Jupiters), the precision of RV measurments has seen substantial improvement over the past decades. Modern instruments like VLT/ESPRESSO (Pepe et al., 2021) are pushing the limits of extreme precision radial velocity measurements towards $\sim$ 10 cm/s. This precision allows for the detection of rocky planets around low-mass stars, exemplified by Proxima Centauri b (Anglada-Escudé et al., 2016). This RV planet is of particular interest, by being a potentially rocky planet in the habitable zone of a nearby M-dwarf star. Additionally, observations over long baselines have extended the discovery space of the RV method towards longer period planets (e.g. Knutson et al., 2014b). The precision of RV instruments is often limited by spectrograph calibration and stellar variability. This makes it much more challenging to search for planets around young and active stars.

Transit photometry

The transit method, spearheaded by missions like Kepler (Borucki et al., 2010; Howell et al., 2014) and TESS (Ricker et al., 2015), has been the most successful method for finding exoplanets. These observatories obtain accurate photometry of many different stars and search for dips in their lightcurves due to the presence of planets that orbit in front of their star, thereby blocking part of the light. Transit lightcurves can be used to measure the radius of the planet, and the observation of multiple transits provides the orbital period. The transit method is, similar to RV, biased towards large, close-in exoplanets as these give the largest and most frequent transit signal. The transit and RV methods are therefore often combined to obtain both the radius and mass of the planet, which can reveal the planet's density and constrain its bulk composition. The first demonstration of the transit method was by Charbonneau et al. (2000), who detected a hot Jupiter around the Sun-like star HD209458, a planet that had already been found using the RV method. Another notable transiting system is TRAPPIST-1, which hosts seven Earth-sized planets orbiting an M-dwarf (Gillon et al., 2017). This system presents a unique opportunity to study rocky planets around a red dwarf star. Some of these planets are located in the habitable zone, the region around a star where liquid water could

exist on the surface of a planet.

1.1.2 Direct imaging

Direct imaging aims to directly take an image of an exoplanet by angularly resolving it from its host star. This is incredibly challenging, as it requires us to overcome the huge contrast between the star and planet at small angular separations. For instance, trying to directly detect reflected light from an Earth-twin around a Sun-like star at a distance of 10 parsecs requires a contrast of $\sim 10^{10}$ at ~100 milliarcseconds. Luckily, the contrast requirements are relaxed when looking for emission from young, massive planets on wide orbits. These young planets are still hot due to remnant energy from their formation. Their spectral energy distribution peaks in the near-infrared, and we typically require contrasts of $\sim 10^5$ to detect them at those wavelengths. The first image of a planetary-mass companion was taken in 2004 using VLT/NACO (Chauvin et al., 2004). This planet, 2M1207 b, orbits a young brown dwarf at a separation of ~55 au, which signficantly decreased the contrast requirements. Subsequently, Marois et al. (2008) revealed a full planetary system around the star HR8799, with four giant planets on wide orbits. The past decade has seen the advent of the first generation of dedicated instruments for direct imaging, such as VLT/SPHERE (Beuzit et al., 2019), Gemini/GPI (Macintosh et al., 2014), Subaru/SCEXAO (Jovanovic et al., 2015), and Magellan/MagAO-X (Males et al., 2018). With these improved instruments and advances in data-processing techniques, a growing number of jovian planets have been directly imaged, some of them shown in Figure 1.2. Some notable detected systems are the β Pictoris system, consisting of two giant planets inside an edge-on circumstellar debris disk (Lagrange et al., 2010, 2019), the PDS 70 system with two accreting protoplanets (Keppler et al., 2018; Haffert et al., 2019), and YSES-1, the first directly imaged multi-planet system around a Sun-like star (Bohn et al., 2020a,b). These exoplanet hunting instruments have conducted surveys to constrain the occurence rates of young wide-orbit super-Jupiters (Nielsen et al., 2019; Vigan et al., 2021). They have given evidence for distinct formation pathways of planetary mass objects and low mass stars. Unfortunately, these surveys have been less successful than initially anticapitated. While most of these early surveys conducted blind searches, the detection rate of direct imaging can be enhanced by using astrometric measurements from Hipparcos and GAIA to identify stars that are likely hosts to massive companions (e.g. Bonavita et al., 2022; Currie et al., 2023; Franson et al., 2023). By identifying objects that are accelerating, one can infer the presence of a potential substellar companion, which can then be confirmed using direct imaging. Because of their brightness and angular separation, young directly-imaged planets are well-suited for detailed characteri-

zation, and are great laboratories for planet formation.

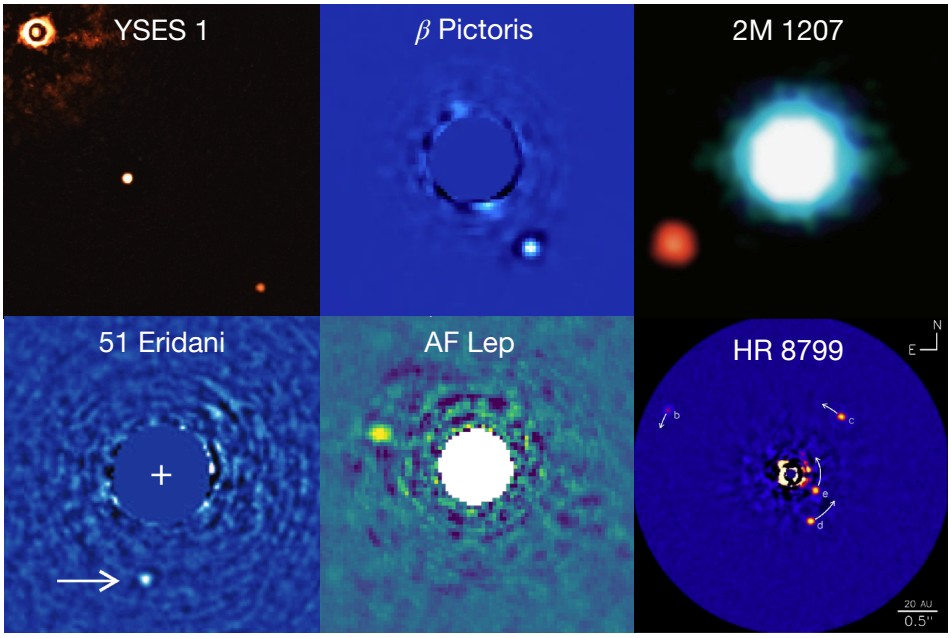

Figure 1.2: Collage of directly imaged exoplanets. References: YSES 1 -Bohn et al. (2020b); β Pictoris - Macintosh et al. (2014); 2M 1207 - Chauvin et al. (2004); 51 Eridani - Macintosh et al. (2015), AF Lep - De Rosa et al. (2023), HR8799 - Marois et al. (2010)

1.2 Characterizing exoplanet atmospheres

While the bulk density of the planet can be obtained from combined RV and transit measurements, there can still be large degeneracies in the planet's properties (Seager et al., 2007). Exoplanet atmospheres provide a crucial window into the planet's chemical composition, thermal structure and dynamics. Additionally, these atmospheres may contain remnant information about the chemical make up of its birthplace, thereby shedding light on its formation history.

1.2.1 Transmission & emission spectroscopy

Transiting planets provide a unique opportunity for atmospheric characterization due their special geometry. During the primary transit, as the exoplanet crosses in front of its host star, starlight passes through the upper layers of the exoplanet's

atmosphere. Based on the composition of this atmosphere, this imprints an additional, wavelength-dependent absorption on the stellar spectrum. Consequently, measuring the transit depth as a function of wavelength allows for the identification of chemical species in the exoplanet's atmosphere (Seager & Sasselov, 2000). The Hubble Space Telescope (HST) has been instrumental in advancing this field, by providing precise low-resolution spectroscopic time series of stars with transiting exoplanets, without having to deal with absorption from the Earth's atmosphere. Charbonneau et al. (2002) found that the transit depth of the planet HD209458 b was slightly enhanced at the wavelengths of the sodium doublet, which they concluded was the result of absorption from the exoplanet's atmosphere. This marked the first detection of an exoplanet atmosphere. Since then, transmission spectroscopy from space has been used to identify water absorption in a large range of planets (e.g. Kreidberg et al., 2015, 2014a; Wakeford et al., 2017). Additionally, the absence of these water features has been used to show that exoplanets can also have clouds or hazes (e.g. Kreidberg et al., 2014b; Knutson et al., 2014a). The presence of excess hydrogen or helium absorption before or after the transit can also be used to probe atmospheric escape (e.g. Vidal-Madjar et al., 2003; Ehrenreich et al., 2015; Spake et al., 2018).

The James Webb Space Telescope (JWST) has majorly enhanced the possibilities of transmission spectroscopy, due to its larger light collecting power and superior wavelength coverage. This extended wavelength range allows for the detection of a much larger variety of chemical species in the atmospheres of these planets. It has for example been used to detect CO_2 in the atmosphere of the bloated warm Neptune WASP-39b (Alderson et al., 2023; Rustamkulov et al., 2023), and to find the photochemical product SO_2 in its atmosphere (Tsai et al., 2023). Additionally, it has been used to find methane in the atmospheres of WASP-80b and K2-18b (Bell et al., 2023; Madhusudhan et al., 2023), which had so far not been conclusively seen in transmission spectra. Transit observations of rocky planets around M-dwarfs with JWST are unfortunately dominated by stellar inhomogeneities, limiting its capability to characterize such planets (e.g. Moran et al., 2023).

Emission spectroscopy, on the other hand, compares the total flux of the system before, after, and during its secondary eclipse, when the exoplanet passes behind its host star (e.g. Deming et al., 2005; Charbonneau et al., 2005). In this scenario, we observe the additional (near-)infrared radiation emitted by the exoplanet. This emission can again be used to identify absorption from chemical species in the exoplanet's atmosphere (e.g. Grillmair et al., 2008). Additionally, it can be used to probe the temperature structure on the daysides of these planets, and infer the presence of potential thermal inversions (e.g. Knutson et al., 2008).

Measuring the light curve over a full orbital period, so-called phase curves, allows for the identification of the longitudinal temperature distribution of the exoplanet (e.g. Stevenson et al., 2014; Demory et al., 2016). This technique can be used to infer the efficiency of the heat transport from the day- to the nightside of the planet, which can constrain the presence or absence of an atmosphere on rocky planets (Kreidberg et al., 2019; Zieba et al., 2023).

1.2.2 High-resolution Doppler spectroscopy

Acquiring accurate wavelength-dependent transit or emission light curves from the ground is challenging. This is because we have to deal with variable turbulence and absorption from the Earth's atmosphere, which also contains the same chemical species that we are often searching for in the exoplanet's atmosphere. To distinguish between the absorption from the Earth and the exoplanet, we can use the fast orbital motion of close-in planets. This motion induces a Doppler shift of the spectral lines originating from the exoplanet. At high spectral resolution, we can then resolve these lines from the telluric features due to their radial velocity shift. This radial velocity changes significantly over the course of the transit for hot Jupiters, allowing us to further distinguish them from telluric or stellar features, which are stationary over time. This phenomenon is illustrated in Fig. 1.3. We often rely on detrending methods, such as Principal Component Analysis or SysRem (Tamuz et al., 2005), to remove these stationary telluric features. High-resolution spectroscopy (HRS) can be applied both to transmission spectroscopy of transiting planets (Snellen et al., 2008), and emission spectroscopy of both transiting (e.g. Snellen et al., 2010) as well as non-transiting planets (e.g. Brogi et al., 2012; Birkby et al., 2017). Since in HRS the light is dispersed over many channels, the signal-to-noise ratio (S/N) of the individual wavelength bins is strongly decreased. To add up the signal from all spectral lines of a certain species, one can use the cross-correlation technique. This applies a matched filter to the data with a designed template spectrum that includes the species that is being searched for. An additional benefit of HRS is that the individual lines of different species are now resolved, removing degeneracies between chemical species that are present at lower spectral resolution, and allowing for the detection of minor species and isotopologues.

Studies at high spectral resolution in the near-infrared, with instruments such as CRIRES, IGRINS, CARMENES, SPIROU, or GIANO have resulted in the detection of water and carbon monoxide in the atmospheres of various hot Jupiters (e.g. Snellen et al., 2010; Brogi et al., 2012; Birkby et al., 2013; de Kok et al., 2013; Lockwood et al., 2014; Brogi et al., 2014, 2018; Alonso-Floriano et al., 2019; Line et al., 2021)). Recently, evidence for more minor chemical species,

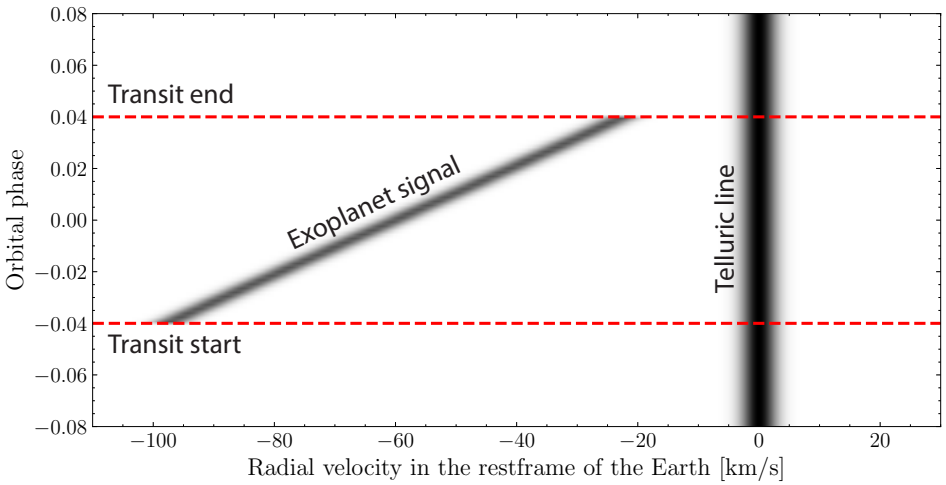

Figure 1.3: Simulation of the noiseless transmission signal of an exoplanet at high spectral resolution, illustrating how high-resolution Doppler spectroscopy can be used to distinguish between spectral lines from a hot Jupiter and telluric lines.

such as HCN, CH_4, NH_3, and C_2H_2 has also been found in the atmospheres of such planets (e.g. Guilluy et al., 2019; Giacobbe et al., 2021). For even hotter planets, so-called ultra-hot Jupiters (UHJs; Parmentier et al. 2018), metals are present in their atomic gaseous form in their atmospheres, and have been detected in the atmospheres of many UHJs using optical high-resolution spectrographs such as ESPRESSO, HARPS and MAROON-X (e.g. Hoeijmakers et al., 2018b; Casasayas-Barris et al., 2019; Kasper et al., 2021a; Kesseli et al., 2022). Some of these metals, such as iron, are strong optical absorbers and, together with species such as TiO (Nugroho et al., 2017; Prinoth et al., 2022) and VO (Pelletier et al., 2023), are thought to be the origin of thermal inversions that are seen in these planets (Fortney et al., 2008). Abundance ratios of refractory elements can be used as probes for the formation of such planets (Lothringer et al., 2021). HRS can also be used to probe atmospheric escape of transiting planets, through for example the helium triplet (e.g. Allart et al., 2018; Nortmann et al., 2018). HRS is sensitive to the shape and radial velocity of the spectral lines. This velocity resolution can be used to reveal atmospheric dynamics, such as winds and rotation in the atmosphere of the exoplanet (Snellen et al., 2010; Brogi et al., 2016; Seidel et al., 2020). For fast-rotating planets we can even spectrally resolve their terminators, by using the fact that the signal from one terminator is blueshifted while the signal from the other is redshifted due to the planet's spin-rotation. This has been used to reveal chemical or temperature asymmetries in UHJs (e.g. Ehren-

reich et al., 2020; Kesseli & Snellen, 2021; Prinoth et al., 2022; Gandhi et al., 2023b). A more in-depth review of HRS can be found in Birkby (2018) and Brogi & Birkby (2021).

1.2.3 Spatially resolved spectroscopy

Spatially resolved spectroscopy, or direct imaging spectroscopy, uses the angular separation between the star and planet to directly obtain the emission spectrum of the exoplanet. The advent of instruments that couple adaptive optics with spectrographs opened up the possibility of in-depth characterization of the atmospheres of young widely separated super-Jupiters that have been detected with direct imaging. Moderate resolution integral field spectroscopy with Keck/OSIRIS was used to characterize the atmosphere of HR8799b (Bowler et al., 2010; Barman et al., 2011), and allowed for the identification of water and carbon monoxide absorption in its atmosphere (Konopacky et al., 2013), along with some evidence for methane absorption (Barman et al., 2015). The combined detection of both water and carbon monoxide (or methane) can be used to measure the atmospheric carbon-to-oxygen (C/O) ratio of these young planets. Due to the presence of snowlines in the protoplanetary disk, the C/O ratio depends on the separation at which the planet formed (Öberg et al., 2011). Measuring the C/O ratio can thus give hints about where the planet formed in its protoplanetary disk (e.g. Mollière et al., 2022), assuming the atmospheric C/O ratio is representative of its bulk composition. The C/O ratio has been measured for a increasing number of directly imaged exoplanets (e.g. Ruffio et al., 2021; Hoch et al., 2022), allowing us to start identifying statistical trends in the population (Hoch et al., 2023). More recently, isotopologue abundance ratios have been proposed as an additional tracer of planet formation, and were shown to be accessible in these young self-luminous planets (Zhang et al., 2021). These planets are also excellent laboratories for atmospheric chemistry. The presence or absence of chemical species such as methane can be for example be used to probe chemical (dis)equilibrium in these planets, and the shape of the emission spectrum gives information about the presence of (patchy) clouds in their atmospheres (e.g. Barman et al., 2011; Mollière et al., 2020).

The arrival of first-generation high-contrast imaging instruments have resulted in the acquisition of low-resolution spectra of various directly imaged planets (e.g. Samland et al., 2017; Claudi et al., 2019). These low-resolution spectra, which are mostly used for boosting detection limits, can unfortunately be dominated by large degeneracies between atmospheric parameters and can be heavily biased depending on the exact choices in the data reduction (Nasedkin et al., 2023). Interferometric observations using VLTI/GRAVITY also offer great potential for obtaining moderate resolution spectra of directly imaged planets. The power of

this was demonstrated in GRAVITY Collaboration et al. (2020), where a high signal-to-noise ratio K-band spectrum of β Pic b was obtained. This spectrum was used to find that the planet has a sub-solar C/O ratio and enhanced metallicity, which points towards a formation through core accretion with significant planetesimal enrichment. Spectroscopy of infant protoplanets can also be used to measure accretion signatures and can help to disentangle the planet formation process (Haffert et al., 2019). Unfortunately, near-infrared spectral features from absorption in the atmospheres of these protoplanets appears to hidden by extinction from dust around the protoplanet (Cugno et al., 2021).

At high-spectral resolution, the individual spectral lines are resolved and we can again use the cross-correlation technique to detect species in the planet's atmosphere. This can be used to measure the rotational velocity of the object and determine the length of its day, as was for the first time done for β Pictoris b (Snellen et al., 2014). Since then, the spin-rotation has been measured for a handful of directly imaged planets and brown dwarf companions (e.g. Schwarz et al., 2016; Bryan et al., 2018; Wang et al., 2021; Xuan et al., 2020). Measurements of the spin of the planet can also be used to trace the formation and evolution of the planet, as the planet is expected to spin-up during its contraction. The spin regulation process may differ depending on the formation pathway of the object. A comparison between the distribution of spin-rotation between planets and brown dwarfs can help to determine if these classes of objects form in different ways (Bryan et al., 2018; Wang et al., 2021). This velocity resolution, in combination with high signal-to-noise data, can also be used to derive the 3D distribution of clouds or temperature inhomegeneities in the atmospheres of directly imaged planets and brown dwarfs using Doppler mapping techniques, as was shown for the nearby brown dwarf binary Luhman-16 by Crossfield et al. (2014). Additionally, the RV measurement of the planet that can be obtained with HRS can help break degeneracies in planetary orbits (e.g. Schwarz et al., 2016), or potentially infer the presence of massive exomoons (Ruffio et al., 2023).

The sensitivity and expanded wavelength range of JWST is also revolutionizing the characterization of directly imaged planets. While the gain for close-in planets is smaller due to the longer wavelengths and relatively old coronagraph technology, it is starting to show exciting results for exoplanets on very wide orbits. The exquisitely detailed spectrum obtained of VHS 1256 b was for example used to identify absorption from silicate clouds (Miles et al., 2023) and oxygen isotopes (Gandhi et al., 2023a).

1.2.4 Atmospheric models & retrievals

Initial studies of exoplanet atmospheres were mostly concerned with determining the presence of individual chemical species or deriving the bulk properties of the exoplanet. However, as the quality of our data improves, we try to learn more about their atmosphere. This can be achieved through atmospheric retrieval techniques, which have been used for characterizing both transiting (e.g. Benneke & Seager, 2012; Line et al., 2021), as well as self-luminous exoplanets (e.g. Mollière et al., 2020; Zhang et al., 2021), at all spectral resolutions. Atmospheric retrievals couple a forward model of the exoplanet's atmosphere with an inversion algorithm, commonly a sampler such as MCMC or Nested Sampling, to obtain posterior distributions on the properties of the exoplanet. There are two main approaches for atmospheric retrievals. In the first, one generates a grid of self-consistent models using sophisticated forward models that contain most of the known physics and a low number of free parameters. This grid of models is then compared to the data to derive the properties of the planet. For self-luminous exoplanets, commonly used atmospheric grids are the BT-SETTL (Allard, 2014) and ATMO (Phillips et al., 2020) model grids. A BT-SETTL model spectrum of a directly imaged sub-stellar companion ($T_{\rm eff}$ = 1200 K, $\log(g)$ = 3.5, solar metallicity) is shown in Fig. 1.4 at spectral resolutions ($R = \lambda/\Delta\lambda$) of both 100,000 and 1,000, showing a plethora of molecular absorption features. The second approach, known as a free retrieval, involves minimal priors on the atmosphere, allowing the data to dictate atmospheric properties. This approach offers a high degree of flexibility but may result in physically implausible results if not constrained effectively. While there are many atmospheric modelling and retrieval codes, petitRADTRANS (Mollière et al., 2019) is used throughout this thesis. It requires as input the bulk parameters of the planet, a pressure-temperature profile, a chemistry model, a cloud model, and calculates the emission or transmission spectrum of the planet.

1.3 High-contrast imaging technology

The direct imaging of exoplanets is an extremely challenging task and therefore requires complex, highly-optmized instrumentation. Technological innovations play a pivotal role in advancing our capabilities with direct imaging. In this section, I will discuss the most important technological concepts that allow us to directly image exoplanets.

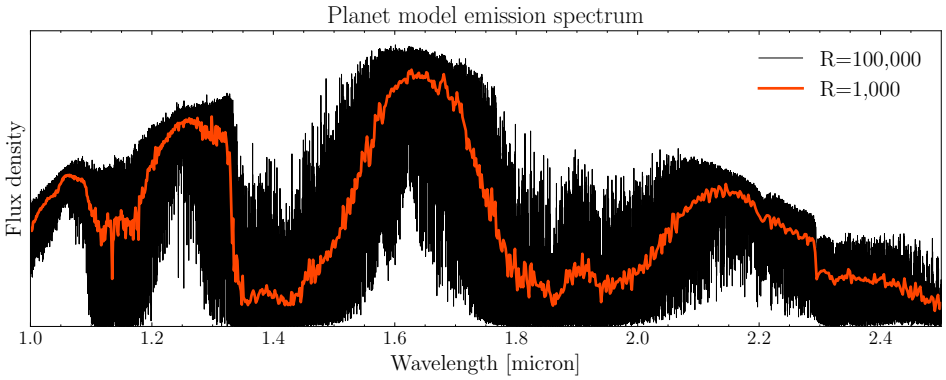

Figure 1.4: BT-SETTL model emission spectrum of a typical directly imaged planet ($T_{\rm eff}$ = 1200 K, log(g) = 3.5, solar metallicity) at spectral resolutions of 1,000 and 100,000, showing a plethora of absorption features from predominantly water and carbon monoxide.

1.3.1 Extreme adaptive optics

At the core of a high-contrast imaging instrument is its Adaptive Optics (AO) system. This AO system tries to counter the blurring effects induced by the Earth's atmosphere that limit the spatial resolution that can be obtained from the ground (Babcock, 1953). AO is crucial for realizing the full potential of large and extremely large telescopes. Fig. 1.5 shows the schematic of an AO system and shows the power of adaptive optics in enhancing the resolution of astronomical observations. AO systems comprise of a wavefront sensor (WFS), one or more deformable mirrors (DM), and real-time control algorithms. The WFS measures the residual distortions introduced by the atmosphere in the incoming starlight, providing a guide for the DM to dynamically correct these in a closed feedback loop. This dynamic correction mitigates atmospheric distortions, allowing the telescope to approach its diffraction limit. The performance of an AO system is often measured by its Strehl ratio, which is defined as the ratio between the peak intensity of the observed point spread function (PSF) to the peak of the ideal diffraction-limited PSF.

The direct imaging of exoplanets requires very deep contrast at small angular separation. To achieve this, we need extreme adaptive optics (XAO; Guyon 2018). While classical AO is mostly concerned with increasing the Strehl ratio up to levels of 10-70% to increase the spatial resolution and light collecting power of e.g. spectrographs, the goal of XAO is to reach very deep contrasts close to the star. XAO requires DMs with a large number of degrees of freedom, with instruments on 8-meter telescopes needing > 1000 actuators. Additionally, XAO

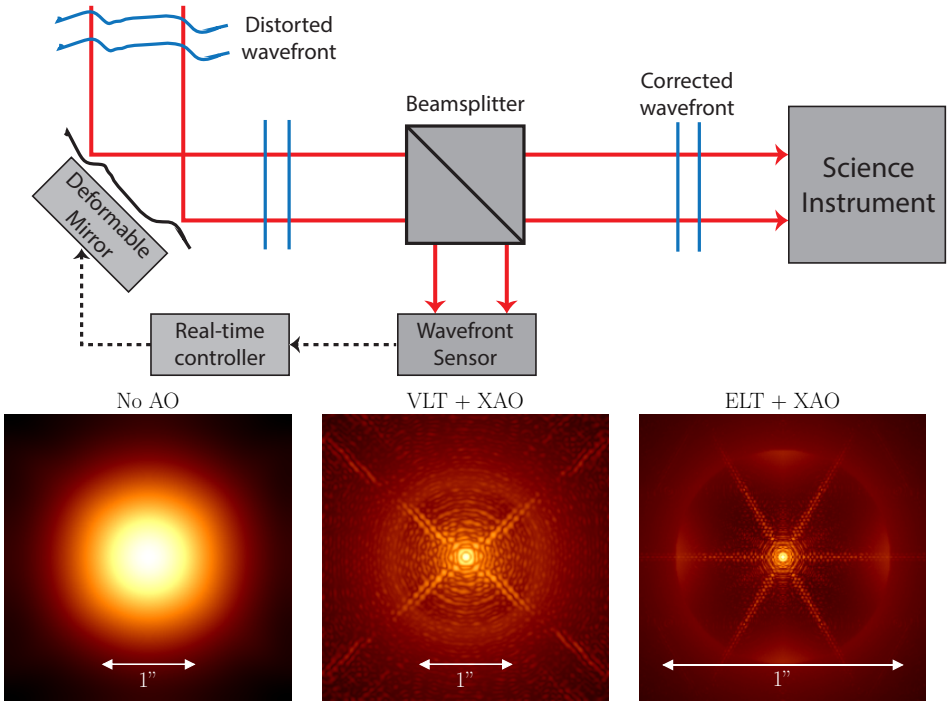

Figure 1.5: Top: Schematic overview of an adaptive optics system. Bottom: Illustration of the gain in angular resolution that can be obtained from extreme adaptive optics. The figures show the long exposure PSFs at 1600 nm for different configurations. Left: Without adaptive optics. Middle: The VLT with XAO. Right: The ELT with XAO. All simulations were conducted using TIPTOP (Neichel et al., 2020).

systems need to run their loop at a frequency of multiple kHz to keep up with the quickly changing atmosphere, which results in strong requirements on the WFS and control algorithm. State-of-the-art XAO systems such as those used in SPHERE and GPI are able to obtain Strehl ratios of ~90% in the H-band.

Wavefront sensing

Different types of WFS exist, each with their strengths and weaknesses. The most commonly used WFS types are illustrated in Fig. 1.6. The Shack-Hartmann wavefront sensor (SHWFS) was the WFS of choice for the first generation of exoplanet hunting instruments (Beuzit et al., 2019; Macintosh et al., 2014). It divides the incoming wavefront into small segments, measuring the tilt of each segment to determine the overall wavefront shape. The preference for next gener-

ation HCI and upgrades of existing instruments is the Pyramid wavefront sensor (PWFS; Ragazzoni 1996), which uses a pyramid-shaped optic to split up the focal plane. The PWFS is the preferred choice due to its increased sensitivity over the SHWFS (Guyon, 2005; Chambouleyron et al., 2023). The sensitivity of a wavefront sensor describes how efficient the wavefront sensor uses the incoming photons to measure the wavefront. A highly efficient wavefront sensor requires less photons to measure the wavefront, and can subsequently be run at higher frequencies. Finally, the Zernike wavefront sensor (ZWFS) uses a $\pi/2$ phase-shifting dot in the focal plane to interfere the Airy core with the starlight itself (N'Diaye et al., 2013a), transforming the phase fluctuations into intensity fluctuations. This allows for a highly sensitive measurement of the incoming phase. Finally, wavefront sensing in the science focal plane is crucial for mitigating aberrations originating from the non-common path between the WFS and science arm (Jovanovic et al., 2018). These non-common path aberrations (NCPAs) evolve slowly over time and can significantly limit the obtainable contrast (Vigan et al., 2019). To remove these aberrations we have to measure the wavefront aberrations at the science focal plane. There are many different concepts for focal plane wavefront sensing (FPWFS), each of them relying on some form of phase diversity to lift the sign ambiguity that is present in the focal plane (e.g. Baudoz et al., 2006; Codona & Kenworthy, 2013; Wilby et al., 2017; Bos et al., 2019). FPWFS is also crucial for sensing aberrations to which most common WFS are blind, such as the low-wind effect (Milli et al., 2018).

Wavefront reconstruction & control

Given the wavefront sensor measurements, we have to determine the ideal shape of the DM. In classical systems, this computation consists of two parts: First, the wavefront is reconstructed in a chosen modal basis. Common modal bases include the Zernike basis or the Karhunen-Loeve basis. This reconstruction is often done using a matrix-vector multiplication, which is pre-calibrated in the lab using an internal source. Alternatively, it is possible to use more sophisticated reconstruction algorithms based on mathematical models of the WFS (e.g. Frazin, 2018; Shatokhina et al., 2020; Chambouleyron et al., 2024) or data-driven machine learning algorithms (e.g. Landman & Haffert, 2020; Archinuk et al., 2023). This is especially important for the PWFS and ZWFS, as these have a nonlinear response to incoming wavefront aberrations (e.g. Deo et al., 2019). The PWFS is often modulated to increase its linearity, but this comes at the cost of decreased sensitivity and a blindness to petal-piston modes (e.g. Hedglen et al., 2022; Bertrou-Cantou et al., 2022). The second part consists of the temporal control of the DM. Classically, an integral control loop is used to update the shape of the DM. How-

ever, because of the time lag between sensing and correcting the wavefront, this leads to a wind-driven halo in the resulting science images (Cantalloube et al., 2020). The advent of predictive control algorithms promises to significantly improve the achievable contrast by both decreasing this wind driven halo at close inner working angles and temporally decorrelating the residual speckles (Guyon, 2005; Males & Guyon, 2018). A promising approach toward predictive control is the use of self-tuning control laws (e.g. Landman et al., 2021; Haffert et al., 2021; Nousiainen et al., 2022).

1.3.2 Coronagraphy

Once the wavefront has been flattened, we can obtain diffraction-limited images of the star. However, diffraction leads to a PSF that contains a central core surrounded by Airy rings of decreasing intensity. These diffraction rings can still be orders of magnitude brighter than the exoplanet we are trying to image. We therefore have to use coronagraphs, which are optical devices that efficiently block the starlight and its diffraction features, while letting the planet light pass through. Several types of coronagraphs have been developed, each with its advantages. The most commonly used coronagraph architecture is the Lyot Coronagraph (Lyot, 1939), which uses a mask in the focal plane to block out the Airy core, together with a Lyot stop in the subsequent pupil plane to block out most of the diffraction features. Improved versions of the Lyot Coronagraph are the (Phase) Apodized Pupil Lyot Coronagraph (Soummer, 2005; Por, 2020), which use a pre-apodizer in the pupil-plane to reshape the PSF in such a way that the diffraction features can be efficiently removed. This apodization is especially important when working with on-axis telescopes, which have a central obscuration and spiders supporting the secondary mirror. Other commonly used coronagraphs are the (vector) Vortex Coronagraph (Foo et al., 2005; Mawet et al., 2010), and coronagraphs that solely rely on pupil-apodization to shape the PSF, such as the Shaped Pupil Coronagraph (Kasdin et al., 2003) and the (vector) Apodizing Phase Plate coronagraph (Kenworthy et al., 2007; Snik et al., 2012; Doelman et al., 2021). While improving coronagraph technology is crucial for space-based HCI, ground-based systems are more commonly limited by the performance of the AO system.

1.3.3 Post-processing

Even with advanced wavefront control and coronagraphy, residual optical imperfections can leak through the system, resulting in speckles in our science data. Post-processing techniques play a crucial role in removing these residual speckles and revealing faint planetary signals. Post-processing techniques rely on diversi-

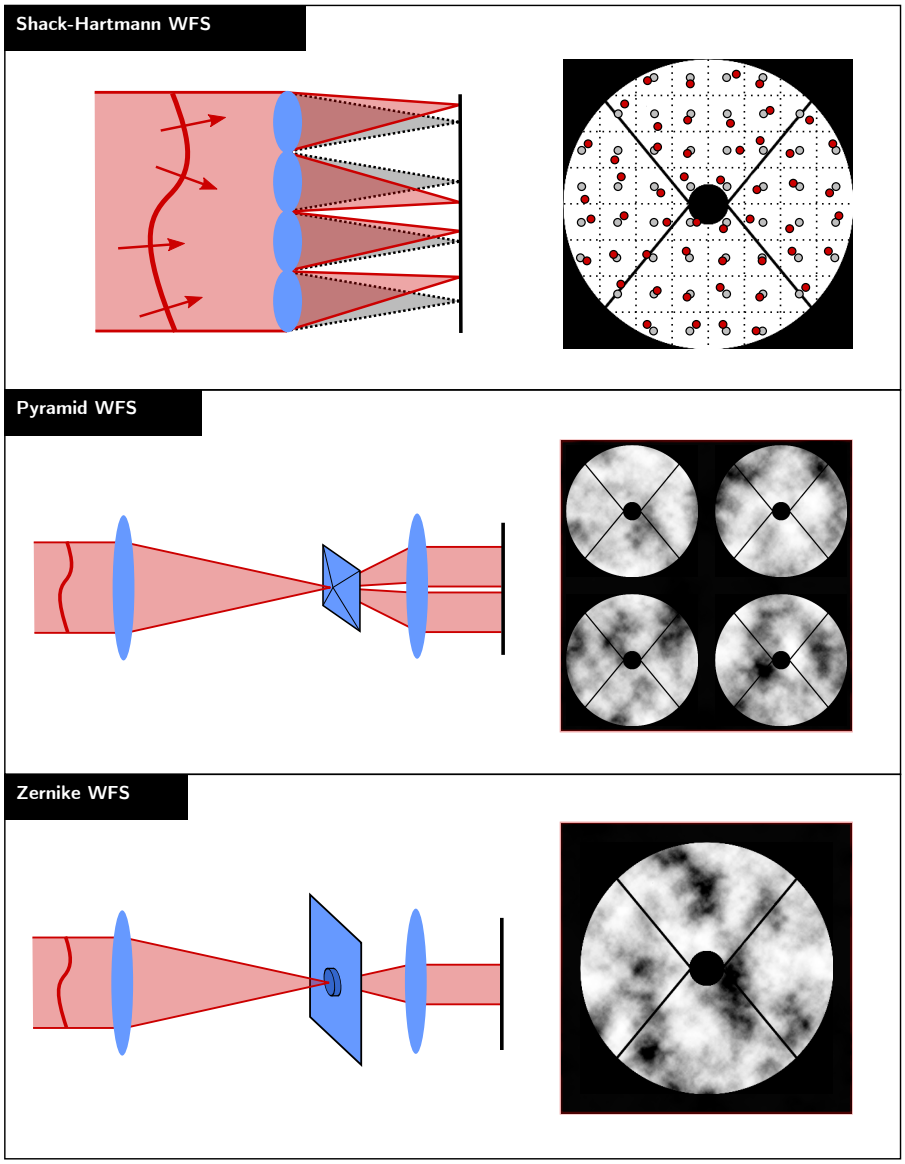

Figure 1.6: Illustration of three most commonly used wavefront sensors in AO Systems: The Shack-Hartmann, Pyramid and Zernike WFS. The optical layout is shown on the left and an example measurement is shown on the right. Image courtesy of Emiel Por.

ties, which are ways in which the planetary signal is different from the stellar signal and its speckles, to enhance the obtainable contrast. The most commonly used post-processing technique is Angular Differential Imaging (ADI; Marois et al. 2006), which leverages the rotation of the sky, and thus any potential planets, to distinguish between light from an astrophysical source and speckles. Another popular technique is Spectral Differential Imaging (SDI; Sparks & Ford 2002), which exploits the difference in spectral signature between star and planet light. While speckles are a diffraction effect and shift outward with increasing wavelength, an astrophysical signal would be at a stationary location over wavelength. Other techniques include Reference star Differential imaging (RDI; Lafrenière et al. 2009; Xie et al. 2022), which uses a library of reference PSFs to subtract the stellar signal, Polarization Differential Imaging (PDI; Kuhn et al. 2001), which utilizes the difference in polarization signature between the stellar signal and that of the planet/disk, and Coherence Differential Imaging (CDI; Bottom et al. 2017), which takes advantage of the interference properties of starlight but not planet and disk light to enhance contrast.

High-resolution spectral differential imaging

SDI can also be extended to work at higher spectral resolution (Sparks & Ford, 2002). In this case, we do not only use the diversity that originates from speckles obeying diffraction, but also the distinct spectral features of the planet and stellar signal, to enhance contrast. Since the emission spectra of a planet contains molecular features, which are not present in the spectra of most stars, we can search for signatures of these features in the data. This technique, dubbed molecule mapping in Hoeijmakers et al. (2018a), can be used at both moderate (e.g. Ruffio et al., 2019; Petrus et al., 2021) and high spectral resolution (e.g. Snellen et al., 2014; Wang et al., 2021). At high spectral resolution, we can additionally use the Doppler shift of the planet to distinguish between stellar/telluric features and the signal from the exoplanet. The major advantage of this technique is that it is less affected by speckle noise than other post-processing techniques. This has allowed it to be succesfully used on data from instruments without XAO systems or coronagraphs, such as Keck/OSIRIS, VLT/SINFONI and VLT/CRIRES. An issue with these integral field spectrographs is that these instruments are often limited by the available detector space, as they benefit from a high spatial resolution, high spectral resolution and a large wavelength coverage. SDI at moderate or high- spectral resolution can also help boost the detection limit of protoplanets (Haffert et al., 2019), by searching for distinct accretion signatures.

1.4 This thesis

This thesis consists of two parts: The first part (chapters 2 and 3) uses current instruments to characterize the atmospheres of two of the most accessible types of planets: Ultra-hot Jupiters and widely-separated super-Jupiters. The second part (chapters 4, 5 and 6) describes the development of key technologies that are required to push the direct imaging and characterization of exoplanets to their limits.

Chapter 2: Detection of OH in the atmosphere of an ultra-hot Jupiter

Ultra-hot Jupiters are planets that have dayside temperatures of > 2000 K, where most molecules are thermally dissociated into their atomic counterparts. This leads to a decreased water absorption feature in their transmission spectrum (Madhusudhan et al., 2011; Mansfield et al., 2021). One of the dissociation products of water is the hydroxyl radical (OH). This chapter presents the detection of OH in the atmosphere of the ultra-hot Jupiter WASP-76b. This molecule was found using high-resolution transmission spectroscopy with the CARMENES instrument. The detection of this molecule confirms that water is being thermally dissociated at the terminator of this planet. This dissociation is important when deriving reliable elemental abundance ratios for these types of planets.

Chapter 3: Atmospheric characterization of β Pictoris b at high spectral resolution

Directly imaged super-Jupiters provide a unique laboratory for testing planet formation and migration theories. Adaptive-optics fed high-resolution spectrographs can facilitate in-depth characterization of these planets. One of the best targets for this characterization is the emblematic β Pictoris b. We observed β Pic b using the refurbished CRIRES+ instrument. Using these observations, we were able to detect carbon monoxide and water in its atmosphere and found that it has a sub-solar C/O ratio. Additionally, we measured its spin-rotation to be $v \sin i = 19.9 \pm 1.0$ km/s, which gives a rotation period, or length of day, of 8.7 ± 0.8 hours. Finally, we also demonstrate the majorly improved potential of CRIRES+ over the old CRIRES for such observations.

Chapter 4: Trade-offs in high-contrast integral field spectroscopy

Combining high-contrast imaging with moderate- to high-resolution spectroscopy has the potential to greatly improve the detection capabilites of direct imaging instruments. However, these integral field spectrographs are often limited by the

detector space available. In this chapter, we try to find the optimal instrument for detecting exoplanets with such an instrument. We study the trade-offs between spectral resolution, spectral bandwidth, wavelength range and field of view and derive new relations between the signal-to-noise ratio and these properties. We find that moderate spectral resolutions already provide a significant increase in detection capabilities and that this technique is most beneficial for close-in exoplanets, where we are limited by noise from stellar speckles.

Chapter 5: Optimal design of wavefront sensors

Adaptive optics is the crucial technology for fulfilling the potential of the ELTs. Direct imaging instruments on these ELTs will need to run their XAO loops at multiple kHz to reach their contrast requirements. This means that we need highly efficient wavefront sensors that can accurately measure the wavefront with a minimum number of photons. This chapter reports on the search for an "optimal" wavefront sensor, which uses all the available photons to measure the wavefront. We present optimal designs for a variety of apertures and show that these designs are close to the theoretical limit. Additionally, we explore the possibility of jointly optimizing the sensor and reconstruction algorithm and find that this expands the design space, leading to sensors with a larger dynamic range.

Chapter 6: Wavefront reconstruction with machine learning

On of the main issues with highly-sensitive wavefront sensors, such as the PWFS, is that they become highly nonlinear when operating with a non-diffraction limited PSF. This limits their dynamic range and subsequently the performance of the XAO system on-sky. In this chapter, we report on tests to extend the dynamic range of the unmodulated PWFS by using a nonlinear reconstructor based on convolutional neural networks (CNN). We show that our nonlinear reconstructor can significantly improve the dynamic range of the WFS and leads to better Strehl ratios in closed-loop tests with MagAO-X.

1.5 Outlook

1.5.1 Towards a census of exoplanet atmospheres

Over the next decade, JWST will continue to characterize many transiting exoplanets in depth. With advances in modelling stellar inhomogeneities, it will likely be able to probe the atmospheres of rocky exoplanets. Missions such as ARIEL (Tinetti et al., 2018) will, on the other hand, provide population level statistics

about the chemical composition of larger close-in exoplanets. From the ground, HRS on existing telescopes will further be used to characterize the atmospheres of (ultra-)hot Jupiters and warm Neptunes. After the arrival of the ELTs, instruments such as ELT/METIS (Brandl et al., 2021), ELT/ANDES (Palle et al., 2023), and TMT/MODHIS (Mawet et al., 2019) will push the capabilities of ground-based HRS to smaller planets and more detailed characterization. Combined, all these instruments will provide a comprehensive insight into the composition, chemistry, and atmospheric dynamics of transiting exoplanets, and will help unravel their origin.

The characterization of directly imaged planets will likely also see significant progress over the next decade. The return of VLT/CRIRES+ and the arrival of VLT/ERIS are again providing the VLT with AO-fed high-resolution spectrographs, which will be crucial for surveying the chemical compostions of widely-separated super-Jupiters. Furthermore, the coupling of existing high-contrast imaging instruments with existing high-resolution spectrographs, such as VLT/HiRISE (Vigan et al., 2024), Keck/KPIC (Delorme et al., 2021) and VLT/RISTRETTO (Lovis et al., 2017) will allow for detailed characterization of more close-in directly imaged exoplanets. Population level analysis of elemental and isotopic abundance ratios of these young gas giants will be possible, and will be excellent tests for planet formation theories. Direct imaging will gain even more from the ELTs, as it will both increase the spatial resolution as well as the light collecting power. ELT/METIS (Brandl et al., 2021), with its mid-infrared wavelength coverage, will likely allow for the direct imaging and characterization of rocky planets, while ELT/HARMONI (Thatte et al., 2021), ELT/ANDES, ELT/PCS (Kasper et al., 2021b), and TMT/MODHIS will push the limits of exoplanet characterization in the optical and near-infrared.

1.5.2 Towards imaging Earth-like planets in the habitable zone

Since a special geometry is required for a planet to transit from our point of view, many of the potential close-by Earth-like planets will be missed. Addtionally, an Earth-like planet around a Sun-like star would transit only once every year. Since many transit observations will likely be required to obtain high enough signal-to-noise ratio to detect biosignatures (Serindag & Snellen, 2019; Hardegree-Ullman et al., 2023), this quickly becomes infeasible. On the other hand, direct imaging still has a long way to go to reach the required contrasts for detecting Earth-like planets in reflected light. From the ground, the focus will be on Earth-like planets in the habitable zone of M-dwarfs, due to the relaxed contrast requirements that they provide. A prominent target for this is Proxima Centauri b, which may be detectable with dedicated instruments that combine high-contrast imaging

with high-dispersion spectroscopy on the ELTs (Snellen et al., 2015). AO will be the most crucial technology for ground-based high-contrast imaging. The first generation of exoplanet imaging instruments are currently being upgraded, with SPHERE+ (Boccaletti et al., 2020), GPI 2.0 (Chilcote et al., 2020), and the continual upgrades that are applied to SCExAO and MagAO-X. These upgrades will test technologies that are pivotal for direct imaging on the ELTs, and will push the limits of HCI on 8 meter class telescopes. Crucial technologies include the digging and maintenance of dark-holes using focal-plane wavefront sensing techniques (e.g. Potier et al., 2020; Haffert et al., 2023), predictive control to decrease the temporal wavefront error, and the development of very high-order DMs that are able to run at multiple kHz. Advances in post-processing algorithms using e.g. WFS telemetry also promises to provide significant gains (Guyon et al., 2021). If these technologies are developed succesfully, instruments such as ELT/PCS, TMT/PSI (Fitzgerald et al., 2022), and GMT/GMagAO-X (Males et al., 2022), should be able detect rocky planets in the habitable zones of the nearest M-dwarfs, and search for biosignatures in their atmospheres.

From space, the Nancy Grace Roman Space Telescope will be the first test of a dedicated high-contrast imaging instrument in space (Kasdin et al., 2020). In the more distant future, NASA's Habitable Worlds Observatory (HWO) is a planned space-based telescope with the main goal of directly imaging Earth-like planets in the habitable zone of Sun-like stars, and identifying biosignatures in their atmosphere. This will require contrasts of $\sim 10^{-10}$ at a few λ/D, and efforts are being made to develop and test coronagraph and wavefront control technologies to reach these contrasts, and test these on testbeds (e.g. N'Diaye et al., 2013b; Baxter et al., 2021).

The combination of all these upcoming facilities may help answer one of the biggest questions: Are we alone in the universe?

References

Alderson, L., Wakeford, H. R., Alam, M. K., et al. 2023, Nature, 614, 664, doi: 10.1038/s41586-022-05591-3

Allard, F. 2014, in Exploring the Formation and Evolution of Planetary Systems, ed. M. Booth, B. C. Matthews, & J. R. Graham, Vol. 299, 271–272, doi: 10.1017/S1743921313008545

Allart, R., Bourrier, V., Lovis, C., et al. 2018, Science, 362, 1384, doi: 10.1126/science.aat5879

Alonso-Floriano, F. J., Sánchez-López, A., Snellen, I. A. G., et al. 2019, A&A, 621, A74, doi: 10.1051/0004-6361/201834339

Anglada-Escudé, G., Amado, P. J., Barnes, J., et al. 2016, Nature, 536, 437, doi: 10.1038/nature19106

Archinuk, F., Hafeez, R., Fabbro, S., Teimoorinia, H., & Véran, J.-P. 2023, Journal of Astronomical Telescopes, Instruments, and Systems, 9, 049005, doi: 10.1117/1.JATIS.9.4.049005

Babcock, H. W. 1953, PASP, 65, 229, doi: 10.1086/126606

Baranne, A., Queloz, D., Mayor, M., et al. 1996, A&AS, 119, 373

Barman, T. S., Konopacky, Q. M., Macintosh, B., & Marois, C. 2015, ApJ, 804, 61, doi: 10.1088/0004-637X/804/1/61

Barman, T. S., Macintosh, B., Konopacky, Q. M., & Marois, C. 2011, ApJ, 733, 65, doi: 10.1088/0004-637X/733/1/65

Baudoz, P., Boccaletti, A., Baudrand, J., & Rouan, D. 2006, in IAU Colloq. 200: Direct Imaging of Exoplanets: Science & Techniques, ed. C. Aime & F. Vakili, 553–558, doi: 10.1017/S174392130600994X

Baxter, W., Potier, A., Ruane, G., & Mejia Prada, C. 2021, in Society of Photo-Optical Instrumentation Engineers (SPIE) Conference Series, Vol. 11823, Techniques and Instrumentation for Detection of Exoplanets X, ed. S. B. Shaklan & G. J. Ruane, 118231S, doi: 10.1117/12.2601432

Bean, J. L., Raymond, S. N., & Owen, J. E. 2021, Journal of Geophysical Research (Planets), 126, e06639, doi: 10.1029/2020JE006639

Bell, T. J., Welbanks, L., Schlawin, E., et al. 2023, Nature, 623, 709, doi: 10.1038/s41586-023-06687-0

Benneke, B., & Seager, S. 2012, ApJ, 753, 100, doi: 10.1088/0004-637X/753/2/100

Bertrou-Cantou, A., Gendron, E., Rousset, G., et al. 2022, A&A, 658, A49, doi: 10.1051/0004-6361/202141632

Beuzit, J. L., Vigan, A., Mouillet, D., et al. 2019, A&A, 631, A155, doi: 10.1051/0004-6361/201935251

Birkby, J. L. 2018, arXiv e-prints, arXiv:1806.04617, doi: 10.48550/arXiv.1806.04617

Birkby, J. L., de Kok, R. J., Brogi, M., et al. 2013, MNRAS, 436, L35, doi: 10.1093/mnrasl/slt107

Birkby, J. L., de Kok, R. J., Brogi, M., Schwarz, H., & Snellen, I. A. G. 2017, AJ, 153, 138, doi: 10.3847/1538-3881/aa5c87

Boccaletti, A., Chauvin, G., Mouillet, D., et al. 2020, arXiv e-prints, arXiv:2003.05714.

https://arxiv.org/abs/2003.05714
Bohn, A. J., Kenworthy, M. A., Ginski, C., et al. 2020a, MNRAS, 492, 431, doi: 10.1093/mnras/stz3462
—. 2020b, ApJ, 898, L16, doi: 10.3847/2041-8213/aba27e
Bonavita, M., Fontanive, C., Gratton, R., et al. 2022, MNRAS, 513, 5588, doi: 10.1093/mnras/stac1250
Borucki, W. J., Koch, D., Basri, G., et al. 2010, Science, 327, 977, doi: 10.1126/science.1185402
Bos, S. P., Doelman, D. S., Lozi, J., et al. 2019, A&A, 632, A48, doi: 10.1051/0004-6361/201936062
Bottom, M., Wallace, J. K., Bartos, R. D., Shelton, J. C., & Serabyn, E. 2017, MNRAS, 464, 2937, doi: 10.1093/mnras/stw2544
Bowler, B. P., Liu, M. C., Dupuy, T. J., & Cushing, M. C. 2010, ApJ, 723, 850, doi: 10.1088/0004-637X/723/1/850
Brandl, B., Bettonvil, F., van Boekel, R., et al. 2021, The Messenger, 182, 22, doi: 10.18727/0722-6691/5218
Brogi, M., & Birkby, J. 2021, in ExoFrontiers; Big Questions in Exoplanetary Science, ed. N. Madhusudhan, 8–1, doi: 10.1088/2514-3433/abfa8fch8
Brogi, M., de Kok, R. J., Albrecht, S., et al. 2016, ApJ, 817, 106, doi: 10.3847/0004-637X/817/2/106
Brogi, M., de Kok, R. J., Birkby, J. L., Schwarz, H., & Snellen, I. A. G. 2014, A&A, 565, A124, doi: 10.1051/0004-6361/201423537
Brogi, M., Giacobbe, P., Guilluy, G., et al. 2018, A&A, 615, A16, doi: 10.1051/0004-6361/201732189
Brogi, M., Snellen, I. A. G., de Kok, R. J., et al. 2012, Nature, 486, 502, doi: 10.1038/nature11161
Bryan, M. L., Benneke, B., Knutson, H. A., Batygin, K., & Bowler, B. P. 2018, Nature Astronomy, 2, 138, doi: 10.1038/s41550-017-0325-8
Cantalloube, F., Farley, O. J. D., Milli, J., et al. 2020, A&A, 638, A98, doi: 10.1051/0004-6361/201937397
Casasayas-Barris, N., Pallé, E., Yan, F., et al. 2019, A&A, 628, A9, doi: 10.1051/0004-6361/201935623
Chambouleyron, V., Fauvarque, O., Plantet, C., et al. 2023, A&A, 670, A153, doi: 10.1051/0004-6361/202245351
Chambouleyron, V., Sengupta, A., Salama, M., et al. 2024, A&A, 681, A48, doi: 10.1051/0004-6361/202347220
Charbonneau, D., Brown, T. M., Latham, D. W., & Mayor, M. 2000, ApJ, 529, L45, doi: 10.1086/312457
Charbonneau, D., Brown, T. M., Noyes, R. W., & Gilliland, R. L. 2002, ApJ, 568, 377, doi: 10.1086/338770
Charbonneau, D., Allen, L. E., Megeath, S. T., et al. 2005, ApJ, 626, 523, doi: 10.1086/429991
Chauvin, G., Lagrange, A. M., Dumas, C., et al. 2004, A&A, 425, L29, doi: 10.1051/0004-6361:200400056
Chilcote, J., Konopacky, Q., De Rosa, R. J., et al. 2020, in Society of Photo-Optical

Instrumentation Engineers (SPIE) Conference Series, Vol. 11447, Ground-based and Airborne Instrumentation for Astronomy VIII, ed. C. J. Evans, J. J. Bryant, & K. Motohara, 114471S, doi: 10.1117/12.2562578

Claudi, R., Maire, A. L., Mesa, D., et al. 2019, A&A, 622, A96, doi: 10.1051/0004-6361/201833990

Codona, J. L., & Kenworthy, M. 2013, ApJ, 767, 100, doi: 10.1088/0004-637X/767/2/100

Crossfield, I. J. M., Biller, B., Schlieder, J. E., et al. 2014, Nature, 505, 654, doi: 10.1038/nature12955

Cugno, G., Patapis, P., Stolker, T., et al. 2021, A&A, 653, A12, doi: 10.1051/0004-6361/202140632

Currie, T., Brandt, G. M., Brandt, T. D., et al. 2023, Science, 380, 198, doi: 10.1126/science.abo6192

de Kok, R. J., Brogi, M., Snellen, I. A. G., et al. 2013, A&A, 554, A82, doi: 10.1051/0004-6361/201321381

De Rosa, R. J., Nielsen, E. L., Wahhaj, Z., et al. 2023, A&A, 672, A94, doi: 10.1051/0004-6361/202345877

Delorme, J.-R., Jovanovic, N., Echeverri, D., et al. 2021, Journal of Astronomical Telescopes, Instruments, and Systems, 7, 035006, doi: 10.1117/1.JATIS.7.3.035006

Deming, D., Seager, S., Richardson, L. J., & Harrington, J. 2005, Nature, 434, 740, doi: 10.1038/nature03507

Demory, B.-O., Gillon, M., de Wit, J., et al. 2016, Nature, 532, 207, doi: 10.1038/nature17169

Deo, V., Gendron, É., Rousset, G., et al. 2019, A&A, 629, A107, doi: 10.1051/0004-6361/201935847

Doelman, D. S., Snik, F., Por, E. H., et al. 2021, Appl. Opt., 60, D52, doi: 10.1364/AO.422155

Ehrenreich, D., Bourrier, V., Wheatley, P. J., et al. 2015, Nature, 522, 459, doi: 10.1038/nature14501

Ehrenreich, D., Lovis, C., Allart, R., et al. 2020, Nature, 580, 597, doi: 10.1038/s41586-020-2107-1

Fitzgerald, M. P., Sallum, S., Millar-Blanchaer, M. A., et al. 2022, in Society of Photo-Optical Instrumentation Engineers (SPIE) Conference Series, Vol. 12184, Ground-based and Airborne Instrumentation for Astronomy IX, ed. C. J. Evans, J. J. Bryant, & K. Motohara, 1218426, doi: 10.1117/12.2630410

Foo, G., Palacios, D. M., & Swartzlander, Grover A., J. 2005, Optics Letters, 30, 3308, doi: 10.1364/OL.30.003308

Fortney, J. J., Lodders, K., Marley, M. S., & Freedman, R. S. 2008, ApJ, 678, 1419, doi: 10.1086/528370

Franson, K., Bowler, B. P., Zhou, Y., et al. 2023, ApJ, 950, L19, doi: 10.3847/2041-8213/acd6f6

Frazin, R. A. 2018, Journal of the Optical Society of America A, 35, 594, doi: 10.1364/JOSAA.35.000594

Gandhi, S., de Regt, S., Snellen, I., et al. 2023a, ApJ, 957, L36, doi: 10.3847/2041-8213/ad07e2

Gandhi, S., Kesseli, A., Zhang, Y., et al. 2023b, AJ, 165, 242, doi: 10.3847/1538-3881/accd65
Giacobbe, P., Brogi, M., Gandhi, S., et al. 2021, Nature, 592, 205, doi: 10.1038/s41586-021-03381-x
Gillon, M., Triaud, A. H. M. J., Demory, B.-O., et al. 2017, Nature, 542, 456, doi: 10.1038/nature21360
GRAVITY Collaboration, Nowak, M., Lacour, S., et al. 2020, A&A, 633, A110, doi: 10.1051/0004-6361/201936898
Grillmair, C. J., Burrows, A., Charbonneau, D., et al. 2008, Nature, 456, 767, doi: 10.1038/nature07574
Guilluy, G., Sozzetti, A., Brogi, M., et al. 2019, A&A, 625, A107, doi: 10.1051/0004-6361/201834615
Guyon, O. 2005, The Astrophysical Journal, 629, 592
Guyon, O. 2018, ARA&A, 56, 315, doi: 10.1146/annurev-astro-081817-052000
Guyon, O., Norris, B., Martinod, M.-A., et al. 2021, in Society of Photo-Optical Instrumentation Engineers (SPIE) Conference Series, Vol. 11823, Techniques and Instrumentation for Detection of Exoplanets X, ed. S. B. Shaklan & G. J. Ruane, 1182318, doi: 10.1117/12.2594885
Haffert, S. Y., Bohn, A. J., de Boer, J., et al. 2019, Nature Astronomy, 3, 749, doi: 10.1038/s41550-019-0780-5
Haffert, S. Y., Males, J. R., Close, L. M., et al. 2021, Journal of Astronomical Telescopes, Instruments, and Systems, 7, 029001, doi: 10.1117/1.JATIS.7.2.029001
Haffert, S. Y., Males, J. R., Ahn, K., et al. 2023, A&A, 673, A28, doi: 10.1051/0004-6361/202244960
Hardegree-Ullman, K. K., Apai, D., Bergsten, G. J., Pascucci, I., & López-Morales, M. 2023, AJ, 165, 267, doi: 10.3847/1538-3881/acd1ec
Hedglen, A. D., Close, L. M., Haffert, S. Y., et al. 2022, Journal of Astronomical Telescopes, Instruments, and Systems, 8, 021515, doi: 10.1117/1.JATIS.8.2.021515
Hoch, K. K. W., Konopacky, Q. M., Barman, T. S., et al. 2022, AJ, 164, 155, doi: 10.3847/1538-3881/ac84d4
Hoch, K. K. W., Konopacky, Q. M., Theissen, C. A., et al. 2023, AJ, 166, 85, doi: 10.3847/1538-3881/ace442
Hoeijmakers, H. J., Schwarz, H., Snellen, I. A. G., et al. 2018a, A&A, 617, A144, doi: 10.1051/0004-6361/201832902
Hoeijmakers, H. J., Ehrenreich, D., Heng, K., et al. 2018b, Nature, 560, 453, doi: 10.1038/s41586-018-0401-y
Howell, S. B., Sobeck, C., Haas, M., et al. 2014, PASP, 126, 398, doi: 10.1086/676406
Jovanovic, N., Martinache, F., Guyon, O., et al. 2015, PASP, 127, 890, doi: 10.1086/682989
Jovanovic, N., Absil, O., Baudoz, P., et al. 2018, in Society of Photo-Optical Instrumentation Engineers (SPIE) Conference Series, Vol. 10703, Adaptive Optics Systems VI, ed. L. M. Close, L. Schreiber, & D. Schmidt, 107031U, doi: 10.1117/12.2314260
Kasdin, N. J., Vanderbei, R. J., Spergel, D. N., & Littman, M. G. 2003, ApJ, 582, 1147, doi: 10.1086/344751
Kasdin, N. J., Bailey, V. P., Mennesson, B., et al. 2020, in Society of Photo-Optical

Instrumentation Engineers (SPIE) Conference Series, Vol. 11443, Space Telescopes and Instrumentation 2020: Optical, Infrared, and Millimeter Wave, ed. M. Lystrup & M. D. Perrin, 114431U, doi: 10.1117/12.2562997

Kasper, D., Bean, J. L., Line, M. R., et al. 2021a, ApJ, 921, L18, doi: 10.3847/2041-8213/ac30e1

Kasper, M., Cerpa Urra, N., Pathak, P., et al. 2021b, The Messenger, 182, 38, doi: 10.18727/0722-6691/5221

Kenworthy, M. A., Codona, J. L., Hinz, P. M., et al. 2007, ApJ, 660, 762, doi: 10.1086/513596

Keppler, M., Benisty, M., Müller, A., et al. 2018, A&A, 617, A44, doi: 10.1051/0004-6361/201832957

Kesseli, A. Y., & Snellen, I. A. G. 2021, ApJ, 908, L17, doi: 10.3847/2041-8213/abe047

Kesseli, A. Y., Snellen, I. A. G., Casasayas-Barris, N., Mollière, P., & Sánchez-López, A. 2022, AJ, 163, 107, doi: 10.3847/1538-3881/ac4336

Knutson, H. A., Benneke, B., Deming, D., & Homeier, D. 2014a, Nature, 505, 66, doi: 10.1038/nature12887

Knutson, H. A., Charbonneau, D., Allen, L. E., Burrows, A., & Megeath, S. T. 2008, ApJ, 673, 526, doi: 10.1086/523894

Knutson, H. A., Fulton, B. J., Montet, B. T., et al. 2014b, ApJ, 785, 126, doi: 10.1088/0004-637X/785/2/126

Konopacky, Q. M., Barman, T. S., Macintosh, B. A., & Marois, C. 2013, Science, 339, 1398, doi: 10.1126/science.1232003

Kreidberg, L., Bean, J. L., Désert, J.-M., et al. 2014a, ApJ, 793, L27, doi: 10.1088/2041-8205/793/2/L27

—. 2014b, Nature, 505, 69, doi: 10.1038/nature12888

Kreidberg, L., Line, M. R., Bean, J. L., et al. 2015, ApJ, 814, 66, doi: 10.1088/0004-637X/814/1/66

Kreidberg, L., Koll, D. D. B., Morley, C., et al. 2019, Nature, 573, 87, doi: 10.1038/s41586-019-1497-4

Kuhn, J. R., Potter, D., & Parise, B. 2001, ApJ, 553, L189, doi: 10.1086/320686

Lafrenière, D., Marois, C., Doyon, R., & Barman, T. 2009, ApJ, 694, L148, doi: 10.1088/0004-637X/694/2/L148

Lagrange, A. M., Bonnefoy, M., Chauvin, G., et al. 2010, Science, 329, 57, doi: 10.1126/science.1187187

Lagrange, A. M., Meunier, N., Rubini, P., et al. 2019, Nature Astronomy, 3, 1135, doi: 10.1038/s41550-019-0857-1

Landman, R., & Haffert, S. Y. 2020, Optics Express, 28, 16644, doi: 10.1364/OE.389465

Landman, R., Haffert, S. Y., Radhakrishnan, V. M., & Keller, C. U. 2021, Journal of Astronomical Telescopes, Instruments, and Systems, 7, 039002, doi: 10.1117/1.JATIS.7.3.039002

Line, M. R., Brogi, M., Bean, J. L., et al. 2021, Nature, 598, 580, doi: 10.1038/s41586-021-03912-6

Lockwood, A. C., Johnson, J. A., Bender, C. F., et al. 2014, ApJ, 783, L29, doi: 10.

1088/2041-8205/783/2/L29
Lothringer, J. D., Rustamkulov, Z., Sing, D. K., et al. 2021, ApJ, 914, 12, doi: 10.3847/1538-4357/abf8a9
Lovis, C., Snellen, I., Mouillet, D., et al. 2017, A&A, 599, A16, doi: 10.1051/0004-6361/201629682
Lyot, B. 1939, Monthly Notices of the Royal Astronomical Society, 99, 580, doi: 10.1093/mnras/99.8.580
Macintosh, B., Graham, J. R., Ingraham, P., et al. 2014, Proceedings of the National Academy of Science, 111, 12661, doi: 10.1073/pnas.1304215111
Macintosh, B., Graham, J. R., Barman, T., et al. 2015, Science, 350, 64, doi: 10.1126/science.aac5891
Madhusudhan, N., Sarkar, S., Constantinou, S., et al. 2023, ApJ, 956, L13, doi: 10.3847/2041-8213/acf577
Madhusudhan, N., Harrington, J., Stevenson, K. B., et al. 2011, Nature, 469, 64, doi: 10.1038/nature09602
Males, J. R., & Guyon, O. 2018, Journal of Astronomical Telescopes, Instruments, and Systems, 4, 019001
Males, J. R., Close, L. M., Miller, K., et al. 2018, in Society of Photo-Optical Instrumentation Engineers (SPIE) Conference Series, Vol. 10703, Adaptive Optics Systems VI, ed. L. M. Close, L. Schreiber, & D. Schmidt, 1070309, doi: 10.1117/12.2312992
Males, J. R., Close, L. M., Haffert, S. Y., et al. 2022, in Society of Photo-Optical Instrumentation Engineers (SPIE) Conference Series, Vol. 12185, Adaptive Optics Systems VIII, ed. L. Schreiber, D. Schmidt, & E. Vernet, 121854J, doi: 10.1117/12.2630619
Mansfield, M., Line, M. R., Bean, J. L., et al. 2021, Nature Astronomy, 5, 1224, doi: 10.1038/s41550-021-01455-4
Marois, C., Lafrenière, D., Doyon, R., Macintosh, B., & Nadeau, D. 2006, ApJ, 641, 556, doi: 10.1086/500401
Marois, C., Macintosh, B., Barman, T., et al. 2008, Science, 322, 1348, doi: 10.1126/science.1166585
Marois, C., Zuckerman, B., Konopacky, Q. M., Macintosh, B., & Barman, T. 2010, Nature, 468, 1080, doi: 10.1038/nature09684
Mawet, D., Serabyn, E., Liewer, K., et al. 2010, ApJ, 709, 53, doi: 10.1088/0004-637X/709/1/53
Mawet, D., Fitzgerald, M., Konopacky, Q., et al. 2019, in Bulletin of the American Astronomical Society, Vol. 51, 134, doi: 10.48550/arXiv.1908.03623
Mayor, M., & Queloz, D. 1995, Nature, 378, 355, doi: 10.1038/378355a0
Miles, B. E., Biller, B. A., Patapis, P., et al. 2023, ApJ, 946, L6, doi: 10.3847/2041-8213/acb04a
Milli, J., Kasper, M., Bourget, P., et al. 2018, in Society of Photo-Optical Instrumentation Engineers (SPIE) Conference Series, Vol. 10703, Adaptive Optics Systems VI, ed. L. M. Close, L. Schreiber, & D. Schmidt, 107032A, doi: 10.1117/12.2311499
Mollière, P., Wardenier, J. P., van Boekel, R., et al. 2019, A&A, 627, A67, doi: 10.1051/0004-6361/201935470
Mollière, P., Stolker, T., Lacour, S., et al. 2020, A&A, 640, A131, doi: 10.1051/0004-6361/202038325

Mollière, P., Molyarova, T., Bitsch, B., et al. 2022, ApJ, 934, 74, doi: 10.3847/1538-4357/ac6a56
Moran, S. E., Stevenson, K. B., Sing, D. K., et al. 2023, ApJ, 948, L11, doi: 10.3847/2041-8213/accb9c
Nasedkin, E., Mollière, P., Wang, J., et al. 2023, A&A, 678, A41, doi: 10.1051/0004-6361/202346585
N'Diaye, M., Dohlen, K., Fusco, T., & Paul, B. 2013a, A&A, 555, A94, doi: 10.1051/0004-6361/201219797
N'Diaye, M., Choquet, E., Pueyo, L., et al. 2013b, in Society of Photo-Optical Instrumentation Engineers (SPIE) Conference Series, Vol. 8864, Techniques and Instrumentation for Detection of Exoplanets VI, ed. S. Shaklan, 88641K, doi: 10.1117/12.2023718
Neichel, B., Beltramo-Martin, O., Plantet, C., et al. 2020, in Society of Photo-Optical Instrumentation Engineers (SPIE) Conference Series, Vol. 11448, Adaptive Optics Systems VII, ed. L. Schreiber, D. Schmidt, & E. Vernet, 114482T, doi: 10.1117/12.2561533
Nielsen, E. L., De Rosa, R. J., Macintosh, B., et al. 2019, AJ, 158, 13, doi: 10.3847/1538-3881/ab16e9
Nortmann, L., Pallé, E., Salz, M., et al. 2018, Science, 362, 1388, doi: 10.1126/science.aat5348
Nousiainen, J., Rajani, C., Kasper, M., et al. 2022, A&A, 664, A71, doi: 10.1051/0004-6361/202243311
Nugroho, S. K., Kawahara, H., Masuda, K., et al. 2017, AJ, 154, 221, doi: 10.3847/1538-3881/aa9433
Öberg, K. I., Murray-Clay, R., & Bergin, E. A. 2011, ApJ, 743, L16, doi: 10.1088/2041-8205/743/1/L16
Palle, E., Biazzo, K., Bolmont, E., et al. 2023, arXiv e-prints, arXiv:2311.17075, doi: 10.48550/arXiv.2311.17075
Parmentier, V., Line, M. R., Bean, J. L., et al. 2018, A&A, 617, A110, doi: 10.1051/0004-6361/201833059
Pelletier, S., Benneke, B., Ali-Dib, M., et al. 2023, Nature, 619, 491, doi: 10.1038/s41586-023-06134-0
Pepe, F., Cristiani, S., Rebolo, R., et al. 2021, A&A, 645, A96, doi: 10.1051/0004-6361/202038306
Petrus, S., Bonnefoy, M., Chauvin, G., et al. 2021, A&A, 648, A59, doi: 10.1051/0004-6361/202038914
Phillips, M. W., Tremblin, P., Baraffe, I., et al. 2020, A&A, 637, A38, doi: 10.1051/0004-6361/201937381
Por, E. H. 2020, ApJ, 888, 127, doi: 10.3847/1538-4357/ab3857
Potier, A., Galicher, R., Baudoz, P., et al. 2020, A&A, 638, A117, doi: 10.1051/0004-6361/202038010
Prinoth, B., Hoeijmakers, H. J., Kitzmann, D., et al. 2022, Nature Astronomy, 6, 449, doi: 10.1038/s41550-021-01581-z
Ragazzoni, R. 1996, Journal of Modern Optics, 43, 289, doi: 10.1080/09500349608232742
Ricker, G. R., Winn, J. N., Vanderspek, R., et al. 2015, Journal of Astronomical Tele-

scopes, Instruments, and Systems, 1, 014003, doi: 10.1117/1.JATIS.1.1.014003
Ruffio, J.-B., Macintosh, B., Konopacky, Q. M., et al. 2019, AJ, 158, 200, doi: 10.3847/1538-3881/ab4594
Ruffio, J.-B., Konopacky, Q. M., Barman, T., et al. 2021, AJ, 162, 290, doi: 10.3847/1538-3881/ac273a
Ruffio, J.-B., Horstman, K., Mawet, D., et al. 2023, AJ, 165, 113, doi: 10.3847/1538-3881/acb34a
Rustamkulov, Z., Sing, D. K., Mukherjee, S., et al. 2023, Nature, 614, 659, doi: 10.1038/s41586-022-05677-y
Samland, M., Mollière, P., Bonnefoy, M., et al. 2017, A&A, 603, A57, doi: 10.1051/0004-6361/201629767
Schwarz, H., Ginski, C., de Kok, R. J., et al. 2016, A&A, 593, A74, doi: 10.1051/0004-6361/201628908
Seager, S., Kuchner, M., Hier-Majumder, C. A., & Militzer, B. 2007, ApJ, 669, 1279, doi: 10.1086/521346
Seager, S., & Sasselov, D. D. 2000, ApJ, 537, 916, doi: 10.1086/309088
Seidel, J. V., Ehrenreich, D., Pino, L., et al. 2020, A&A, 633, A86, doi: 10.1051/0004-6361/201936892
Serindag, D. B., & Snellen, I. A. G. 2019, ApJ, 871, L7, doi: 10.3847/2041-8213/aafa1f
Shatokhina, I., Hutterer, V., & Ramlau, R. 2020, Journal of Astronomical Telescopes, Instruments, and Systems, 6, 010901, doi: 10.1117/1.JATIS.6.1.010901
Snellen, I., de Kok, R., Birkby, J. L., et al. 2015, A&A, 576, A59, doi: 10.1051/0004-6361/201425018
Snellen, I. A. G., Albrecht, S., de Mooij, E. J. W., & Le Poole, R. S. 2008, A&A, 487, 357, doi: 10.1051/0004-6361:200809762
Snellen, I. A. G., Brandl, B. R., de Kok, R. J., et al. 2014, Nature, 509, 63, doi: 10.1038/nature13253
Snellen, I. A. G., de Kok, R. J., de Mooij, E. J. W., & Albrecht, S. 2010, Nature, 465, 1049, doi: 10.1038/nature09111
Snik, F., Otten, G., Kenworthy, M., et al. 2012, in Society of Photo-Optical Instrumentation Engineers (SPIE) Conference Series, Vol. 8450, Modern Technologies in Space- and Ground-based Telescopes and Instrumentation II, ed. R. Navarro, C. R. Cunningham, & E. Prieto, 84500M, doi: 10.1117/12.926222
Soummer, R. 2005, ApJ, 618, L161, doi: 10.1086/427923
Spake, J. J., Sing, D. K., Evans, T. M., et al. 2018, Nature, 557, 68, doi: 10.1038/s41586-018-0067-5
Sparks, W. B., & Ford, H. C. 2002, ApJ, 578, 543, doi: 10.1086/342401
Stevenson, K. B., Désert, J.-M., Line, M. R., et al. 2014, Science, 346, 838, doi: 10.1126/science.1256758
Tamuz, O., Mazeh, T., & Zucker, S. 2005, MNRAS, 356, 1466, doi: 10.1111/j.1365-2966.2004.08585.x
Thatte, N., Tecza, M., Schnetler, H., et al. 2021, The Messenger, 182, 7, doi: 10.18727/0722-6691/5215
Tinetti, G., Drossart, P., Eccleston, P., et al. 2018, Experimental Astronomy, 46, 135,

doi: 10.1007/s10686-018-9598-x
Tsai, S.-M., Lee, E. K. H., Powell, D., et al. 2023, Nature, 617, 483, doi: 10.1038/s41586-023-05902-2
Vidal-Madjar, A., Lecavelier des Etangs, A., Désert, J. M., et al. 2003, Nature, 422, 143, doi: 10.1038/nature01448
Vigan, A., N'Diaye, M., Dohlen, K., et al. 2019, A&A, 629, A11, doi: 10.1051/0004-6361/201935889
Vigan, A., Fontanive, C., Meyer, M., et al. 2021, A&A, 651, A72, doi: 10.1051/0004-6361/202038107
Vigan, A., El Morsy, M., Lopez, M., et al. 2024, A&A, 682, A16, doi: 10.1051/0004-6361/202348019
Wakeford, H. R., Sing, D. K., Kataria, T., et al. 2017, Science, 356, 628, doi: 10.1126/science.aah4668
Wang, J. J., Ruffio, J.-B., Morris, E., et al. 2021, AJ, 162, 148, doi: 10.3847/1538-3881/ac1349
Wilby, M. J., Keller, C. U., Snik, F., Korkiakoski, V., & Pietrow, A. G. M. 2017, A&A, 597, A112, doi: 10.1051/0004-6361/201628628
Wolszczan, A., & Frail, D. A. 1992, Nature, 355, 145, doi: 10.1038/355145a0
Xie, C., Choquet, E., Vigan, A., et al. 2022, A&A, 666, A32, doi: 10.1051/0004-6361/202243379
Xuan, J. W., Bryan, M. L., Knutson, H. A., et al. 2020, AJ, 159, 97, doi: 10.3847/1538-3881/ab67c4
Zhang, Y., Snellen, I. A. G., Bohn, A. J., et al. 2021, Nature, 595, 370, doi: 10.1038/s41586-021-03616-x
Zieba, S., Kreidberg, L., Ducrot, E., et al. 2023, Nature, 620, 746, doi: 10.1038/s41586-023-06232-z